

Accepted Manuscript

Mechanical properties and real-time damage evaluations of environmental barrier coated SiC/SiC CMCs subjected to tensile loading under thermal gradients

M.P. Appleby, Dongming Zhu, G.N. Morscher

PII: S0257-8972(15)00455-7
DOI: doi: [10.1016/j.surfcoat.2015.07.042](https://doi.org/10.1016/j.surfcoat.2015.07.042)
Reference: SCT 20427

To appear in: *Surface & Coatings Technology*

Received date: 1 May 2015
Revised date: 30 June 2015
Accepted date: 1 July 2015



Please cite this article as: M.P. Appleby, Dongming Zhu, G.N. Morscher, Mechanical properties and real-time damage evaluations of environmental barrier coated SiC/SiC CMCs subjected to tensile loading under thermal gradients, *Surface & Coatings Technology* (2015), doi: [10.1016/j.surfcoat.2015.07.042](https://doi.org/10.1016/j.surfcoat.2015.07.042)

This is a PDF file of an unedited manuscript that has been accepted for publication. As a service to our customers we are providing this early version of the manuscript. The manuscript will undergo copyediting, typesetting, and review of the resulting proof before it is published in its final form. Please note that during the production process errors may be discovered which could affect the content, and all legal disclaimers that apply to the journal pertain.

Mechanical properties and real-time damage evaluations of environmental barrier coated SiC/SiC CMCs subjected to tensile loading under thermal gradients

M.P. Appleby^{* a,b}, Dongming Zhu^a, G.N. Morscher^b

^a NASA Glenn Research Center, Cleveland, OH 44135, USA

^b Department of Mechanical Engineering, The University of Akron, Akron OH 44325

ABSTRACT

Environmental barrier coating (EBC) coated ceramic matrix composite (CMC) systems are currently being investigated for use as turbine engine hot-section components in extreme environments. In these extreme conditions, it becomes critical to understand material response to environmental exposure and performance under thermo-mechanical loading. Electrical resistance (ER) monitoring has recently been correlated to tensile damage accumulation in SiC/SiC CMCs, and the focus of this study is to extend the use of ER to evaluate high-temperature thermal gradient fracture of EBC/CMC systems. Tensile strength tests were performed at high temperature (1200°C) using a laser-based heat-flux technique. Specimens included an as-produced SiC/SiC CMC and coated SiC/SiC substrate that have been exposed to simulated combustion environments in a high-pressure burner rig. Localized stress-dependent damage was determined using acoustic emission (AE) monitoring and compared to full-field strain mapping using a high-temperature digital image correlation (DIC) technique. The results are compared with in-situ ER monitoring, and post-test inspection of the samples in order to correlate ER response to damage evolution.

1. Introduction

Ceramic matrix composites (CMCs) are currently under development for implementation in next generation turbine engine hot sections. These materials provide increased performance over current nickel-based superalloys due to their inherent low density, and high-temperature durability and strength. Among the numerous CMCs being investigated, silicon carbide (SiC) fiber-reinforced melt-infiltrated (MI) SiC matrix composites have shown increased high temperature strength and capabilities up to 1315°C [1-3]. These properties are attributed to the increased matrix densification of MI composites over alternative SiC/SiC CMC processing routes, such as polymer infiltration and pyrolysis (PIP) and chemical vapor infiltration (CVI). The near fully dense matrix in MI composites increases the ability of the matrix to carry load and decreases routes for environmental attack on the reinforcing fibers. However, the maximum operating temperature is limited due to the relatively high volume fraction (5-10%) of unreacted silicon remaining in the matrix after processing; whose melting point is approximately 1400°C.

One typical advantage of Si-based materials is their excellent high temperature oxidation resistance in dry air. However, in the presence of water vapor containing combustion environments, the protective silica layer formed at elevated temperatures volatilizes leading to rapid surface recession of the material [4-7]. Therefore, new state-of-the-art coatings are needed to not only withstand increased temperature requirements, but high-velocity corrosive combustion gasses as well. To meet this need, a large effort has been made to develop multilayer ceramic coatings known as Environmental Barrier Coatings (EBCs) in order to protect SiC/SiC CMCs and increase component life-time and durability [8-14].

In order for EBC-CMCs to be successfully implemented as structural components, it is critical to gain an improved understanding of damage initiation and progression under turbine

engine stresses, temperatures, and environmental exposure. Many of the turbine engine component applications for EBC-CMCs (turbine engine vanes/blades, combustor liners, etc.) will be subjected to high heat-fluxes and complex stress states caused by asymmetrical thermal/mechanical loading and the use of forced air cooling [15, 16]. Standard testing used for material characterization is therefore incapable of adequately simulating the operating environments proposed for EBC-CMCs. In an effort to investigate ceramic composites and coating systems, a number of specialized testing rigs have been developed [4, 11, 17-21]. Such tests have already been used to illuminate the difference in damage mechanisms under high heat-flux thermal gradient conditions when compared to room temperature or isothermal testing.

Furthermore, it is crucial that various non-destructive evaluation (NDE) techniques be investigated that could provide critical information useful in assessing damage development and material state during complex testing scenarios. Ideally, such techniques would be simple to implement on a material level as well as a structural testing scale. Recent studies have shown the viability of using in-situ modal acoustic emission (AE) and electrical resistance (ER) monitoring of SiC/SiC CMC specimens during room temperature monotonic tensile loading in order to detect damage onset and accumulation in both CVI [22] and MI-CVI matrices [23]. These works were successful in determining a correlation between electrical resistance increase and stress-dependent transverse matrix cracking. However, because EBC-CMCs are intended for high temperature use, investigation of damage mechanisms and stress-rupture at elevated temperatures becomes the critical focus. A recent investigation was performed to evaluate the usefulness of ER monitoring for high temperature creep characterization of EBC coated MI SiC/SiC CMCs under furnace-heating (quasi-isothermal) and laser-heated high heat-flux (thermal gradient) conditions [24]. While this work showed a correlation between time-

dependent strain accumulation and ER increase, it is clear that high temperature electrical response of these systems can be quite convoluted and requires further examination. Therefore, if ER is to be used as a health monitoring technique, a better understanding of the effects of thermal and mechanical loading, as well as environmental effects is necessary.

The present work compares the ER response of coated and uncoated MI-SiC/SiC CMC substrates subjected to exposure to simulated engine environments followed by high-temperature monotonic tensile strength tests in order to assess retained material properties and strength. In-situ modal AE monitoring will be used in order to correlate changes in electrical response with stress-dependent matrix cracking during tensile loading, and to provide insights into material damage state that ER measurements may not be sensitive to. Furthermore, a novel high-temperature digital image correlation (DIC) technique is described that allows for the comparison of high-temperature ER and AE results with localized strain mapping of the specimen gage section during testing.

The primary objective of the present paper is to investigate the feasibility of using ER measurements in high-temperature testing environments, specifically combined high heat-flux and mechanical loading conditions. In addition, the various NDE methods described earlier (ER, AE and DIC) are used to determine and quantify damage onset and accumulation, and CMC degradation due to the simulated engine environment exposure. Finally, evidence of EBC damage onset and failure is presented by post-test AE event waveform analysis.

2. Experimental materials and methods

2.1 Materials

The ceramic composite substrates tested in this study consist of 8 plies of balanced $0^\circ/90^\circ$, 5 harness-satin woven preforms of Hi-Nicalon Type S (HNS) near-stoichiometric SiC

fibers. Using a chemical vapor deposition (CVD) method the fiber preforms were coated with a boron nitride (BN) interphase, followed by a layer of CVI SiC, with final densification by a slurry cast molten silicon melt-infiltration process that results in a reaction bonded Si-SiC matrix material. The 152 mm (6 in) tensile specimens used in this test were machined from the same composite panel manufactured by Hyper-Therm HTC, Inc. (currently Rolls-Royce, Huntington Beach, CA). Details of the two CMC specimens used in this study have been listed in Table I. Note that the fiber volume fraction in the loading direction, f_0 , is calculated by dividing the cross-sectional area of the specimen by the approximate fiber area in the longitudinal direction. The fiber area is estimated as the area of a single fiber, multiplied by the number of fibers in a fiber-tow, number of tows per ply and number of plies in the composite lay-up [25].

Of the CMC tensile specimens, one was coated with a multilayer EBC coating. The coating consisted of a thin bond coat layer to ensure good adhesion to the CMC substrate, followed by a top coat layer for environmental protection. Both layers were deposited to the surface via electron beam-physical vapor deposition (EB-PVD). The bond coat consisted of a newly developed NASA HfO₂-Si composite bond coat, and the top coat was deposited as NASA HfO₂-doped yttrium-gadolinium di-silicate (Yb,Gd)₂Si₂O₇ environmental barrier coating system [26, 27].

2.2 High Pressure Burner Rig Exposure

In order to simulate exposure to harsh engine environments, an existing high pressure burner rig (HPBR) at NASA Glenn Research Center (Cleveland, OH) was used. The HPBR has been used previously for high-temperature environmental durability studies of advanced aircraft materials and coatings. While design, construction and operation can be found elsewhere [4, 7], the HPBR burns jet-fuel and air at user controlled ratios. The burner rig has been significantly

upgraded, and the test conditions (i.e. gas pressures, temperatures and velocities) closely simulate aero-turbine engine environments [28]. The coated and uncoated SiC/SiC specimens were tested in the high pressure burner rig at 1315°C for 30 hours at 10 atm and combustion gas velocities of 200 m/sec in order to evaluate SiC/SiC degradation and the effect of the environmental barrier coating.

2.3 High-Temperature Monotonic Tensile Testing

A specialized testing rig is utilized in order to assess retained high temperature tensile properties post-HPBR exposure. A high power (3.5kW) high heat-flux CO₂ laser is used to asymmetrically heat the material specimens, generating a multi-axial (through-thickness and longitudinal) thermal gradient. A spinning optical system is used to distribute the beam into an approximately 32 mm heated section on the front surface of the specimen. The through-thickness thermal gradient can be increased by the addition of active air-cooling delivered by a shower-jet head aim at the back side of the material. Thermal gradient testing is used in order to more closely simulate the thermal loading conditions expected for many EBC-CMC aero-turbine engine applications. The front and back-side temperatures of the heated zone are monitored using a pair of infrared pyrometers. It should be noted that the front-side temperature measurement refers to either the coating surface or the substrate surface (depending on whether coating is applied), while the back-side measurement is on the opposing, non-heated face. For this study, the samples were heated in order to produce CMC surface temperatures of approximately 1200°C. The tensile specimen is held by ceramic grip inserts (to eliminate electrical interference of the ER measurement) in an electromechanical tensile load frame. Heating of the specimen is carried out under a “no load” condition in which free thermal expansion in the longitudinal

direction is allowed to prevent excessive thermal stresses. Mechanical loading of the specimen is conducted at a rate of 0.127 mm/min. Refer to Figure 1 for details of experimental setup.

Elongation of the laser-heated section is monitored via two separate methods. First, the nominal strain of the gage section is measured using a high-temperature extensometer with a 25.4 mm gage section with a ± 0.5 mm travel. Secondly, a high-temperature DIC technique was used to determine localized strain fields. In order to track the displacement field, a high temperature Y_2O_3 based aerosol paint (ZYP Coatings, Inc., Oak Ridge, TN) was sprayed onto the sample surface prior to specimen heat-up and subsequent tensile testing, forming a random speckle pattern. In order to track the evolution of the strain field, post processing was performed on the DIC images using commercially available DIC software (ARAMIS, GOM Co. Ltd., Germany). The sample was illuminated using two high intensity LED lamps angled toward the area of interest, and a fan was used to reduce heat distortion of the image by mixing the air in front of the heated specimen.

During tensile testing, the electrical resistance of the specimen is monitored using an Agilent 34420A digital multimeter utilizing a four-point probe method to minimize the contribution of contact resistance. Due to the high temperatures of the heated area during testing, the ER electrodes are attached to the material specimen inside the test frame grips. This configuration ensures good contact pressure between electrode and sample, and also prevents exceeding the melting temperature of the copper electrodes. The outer electrodes are attached at the specimen ends, with the inner electrodes attached at 15 mm from the specimen ends (resulting in an inner probe separation distance of approximately 122 mm) as shown in Figure 2. Acoustic emission events were monitored using a Digital Wave Fracture Detector equipped with two wide-band (50 kHz – 2 MHz) sensors attached to the top and bottom of the specimen

(approximately ± 40 mm from coupon centerline), and data was acquired at the rate of 10 MHz when triggered. The location of the AE events was determined by calculation the difference in time of arrival between each sensor.

3. Results and discussion

3.1 Retained properties

The monotonic tensile results for the two composite systems appear in Figure 3. The coated sample was heated to an EBC surface temperature of 1230°C and SiC/SiC substrate back side temperature of 1070°C, and the uncoated sample was heated to SiC/SiC front and back side temperatures of 1200°C and 1010°C respectively. The stress-strain behavior for the two samples is plotted in terms of nominal strain measured by the high temperature extensometer, as well as the change in elongation of two discrete points taken from the DIC mapping at the points of contact of the upper and lower extensometer probes. It is clear that while there is a higher degree of noise in the DIC analysis, both systems are in general agreement in terms of mechanical behavior. Note that the DIC data is offset by the thermal strain induced by specimen heat up, whereas the extensometer data reflects only the mechanical strains.

The differences in retained mechanical properties between the samples are listed in Table II. The uncoated sample exhibits a decreased stiffness and retained ultimate tensile strength when compared to the coated sample. Furthermore, the uncoated sample shows little inelastic deformation and fails far more elastically. The pseudo-plasticity exhibited by the coated sample is indicative of a gradual stress-dependent accumulation of through-thickness, fiber-bridged matrix cracks and associated fiber sliding. That is, if the stress on the matrix exceeds a critical value it is relieved by initiating a crack in a given area. If the interphase material is sufficiently weak, then in the wake of these matrix cracks a zone is created where the bridging fibers and

matrix have debonded and the load is shared between the fibers and matrix via an interfacial friction mechanism [29-31]. Such global load sharing behavior is the desired effect in CMCs in order to engineer some degree of toughness into the material.

The fact that this behavior is not seen in the uncoated sample indicates that the composite properties were severely degraded by environmental exposure to the HPBR. As previously mentioned, rapid surface recession occurs in the composite when exposed to high temperature oxidizing environments (containing both O_2 and CO_2) like the one generated in the burner rig. If the oxidation front reaches the fiber tows and/or there exists an open pathway for the highly oxidative species to reach the fiber tows, a number of reactions can occur resulting in rapid material change. For instance, oxidation of the BN fiber/matrix interphase can result in solid oxidation reaction products which can strongly bond fibers to the matrix or neighboring fibers to each other. These strongly bonded fibers generate localized stress concentrations leading to local fiber failures. Fibers that are exposed to the oxidizing environment may also experience rapid surface recession/volatilization. These degraded fibers will have a decreased cross-sectional area and therefore a decreased load carrying capability [32].

Post-test observations of the fracture surfaces of the CMCs showed a decreased level of fiber pullout in the uncoated sample. This decreased fiber pullout is indicative of the interphase oxidation mechanism described above, and is comparable to results found in previous high-temperature testing of similar SiC/SiC CMC materials [24]. Areas where oxidation products inhibit fiber/matrix debonding and associated sliding result in localized stress concentrations, and along with possible fiber recession, ultimately lead to a much lower composite strain to failure (as seen in Figure 3). It is clear therefore, that the application of the EBC to the SiC/SiC substrate

greatly increased composite durability and retained mechanical properties by limiting the detrimental effects of exposure to the highly oxidizing HPBR environment.

3.2 ER and AE comparison

The variations in electrical responses and acoustic emission behaviors between the coated and uncoated samples are shown in Figure 4a. It should be noted that the AE events considered here are only those that originated from the heated gage-section of the composite, while the events occurring outside this region-of-interest have been discarded. In contrast, the electrical resistance (as stated above) is measured along nearly the entire length of the specimen. Therefore, this lack in spatial resolution in high-temperature in-situ ER should be noted as one of its current disadvantages.

It has been shown that the accumulation of AE energy during tensile loading of MI SiC/SiC composites is directly proportional to stress-dependent, transverse matrix crack accumulation [31]. Hence, the nature of AE energy accumulation is indicative of material damage response. For instance, the AE onset stress has been shown to correspond quite well to the onset of fiber-bridged matrix crack formation and is considered equivalent to the matrix cracking stress (proportional limit). The AE onset stress is defined as the onset of a high rate of high-energy AE events and is determined by extrapolating the steep portion of the cumulative AE curve back to the zero axis [33]. The AE onset stresses for the each sample is listed in Table II. The AE onset stress of the uncoated sample (115 MPa) as opposed to the coated sample (149 MPa) is evidence of surface recession of the uncoated composite (from the HPBR exposure) leading to a reduction in matrix load carrying capacity. Furthermore, the decreased AE energy accumulation in the uncoated sample is likely caused by the development of unbridged matrix cracking due to strongly bonded or weakened fibers.

While the ER response follows an increasing trend similar the cumulative AE energy curve, the electrical behavior of the two samples shows some slightly different behavior. Comparison of the ER responses in Figure 4a of the two different samples can provide further insight into the possible differences in their respective damage morphology. The low stress region of both tests sees very little increase in resistance due to the elastically dominated response of the material at loads below matrix cracking onset. In general, the coated specimen sees a gradual increase in ER that follows the nature of the cumulative AE energy quite closely. However, at elevated stresses when the slope of the AE energy curve begins to decrease (approaching matrix crack saturation), the change in ER continues increasing dramatically. This behavior is more clearly illustrated by plotting the ER versus the normalized cumulative AE energy (i.e. normalized approximate crack density), as shown in Figure 5a. This continued increase in ER is due to the effects of crack opening and fiber sliding that continue even after matrix crack rate changes. That is, although the rate of matrix cracking has decreased, the length of high resistivity fibers that are debonded from the matrix and/or bridging transverse matrix cracks continues to increase. Alternatively, the response of the uncoated sample shows very little increase in electrical resistance for the first approximately 50% of AE energy accumulation (as seen in Figure 5b). The highly localized damage formation of the sample, caused by degradation from environmental exposure, results in the electrical response at low stresses to be dominated by the largely undamaged elastic regions of the composite in between matrix cracks which possess only small crack openings (accounting for the accumulation of AE energy and the corresponding minor change in ER). Elevated stresses lead to an increase in matrix crack formation and crack opening, along with large scale fiber breaks, resulting in a rapid increase in ER just prior to failure.

Figure 4b shows the electrical response of the samples with increasing nominal mechanical strain. The coated and uncoated samples show increases in electrical resistance of 220% and 180% over the entire specimen length, with measured increases in gage-section strain of 0.371% and 0.134% respectively. As is the case of room temperature tensile loading of SiC/SiC composite systems [22-23], the ER increase in these tests appears to be strongly related to damage accumulation. In the case of room temperature tests, the high volume fraction of free silicon in the matrix results in a dominance in electrical conductivity of the Si-SiC matrix material over the more resistive CVI-SiC and BN coated SiC fibers. Therefore, increasing the number of matrix cracks results in smaller lengths of the more conductive undamaged composite, separated by longer lengths of highly resistive fiber-bridged transverse cracks. Such damage would, of course, act to impede the flow of electrical current (i.e. increase the overall electrical resistance) of the composite. The similar ER behavior seen in this study leads to the conclusion that the high temperature tests are controlled by the same mechanism. Recent modeling efforts have considered the CMC as an electrical circuit consisting of a series of resistors representing: bonded composites segments, debonded fiber/matrix regions and matrix cracks bridged solely by the reinforcing fibers [23]. As a result, one potential advantage of in-situ ER is that it is sensitive to both stress-dependent matrix cracking and corresponding increases in composite strain (in the form of relative fiber/matrix displacement in the fiber/matrix debond and fiber-bridged matrix crack regions). Furthermore, the residual increase of ER that would be associated with permanent plastic deformation leads to the possibility that, unlike strain or AE monitoring, ER measurements could be used as a scheduled inspection technique. Therefore, rapid or excessive increase in the periodically measured electrical resistance of a SiC/SiC structure could be used for component lifing as it has been shown to correlate with large scale composite damage.

3.3 AE waveform analysis

The principle of AE monitoring is that the fracture energy of a material is released as elastic waves that can be detected by the AE sensors. One benefit of modal AE over traditional AE monitoring is the ability to perform post-processing on individual AE event waveforms in order to extract AE event location, energy and frequency content. The location of a given AE event (x) is estimated by the difference in times of arrival (determined by a minimum threshold crossing) of the AE wave at the top (t_{top}) and bottom (t_{bottom}) sensors:

$$x = v/2 (t_{bottom} - t_{top})$$

AE wave velocity (v) was determined prior to high-temperature tensile testing by performing pencil lead breaks at various locations along the specimen length in order to manually generate AE sources. Because material damage will decrease the speed at which sound travels through the material, the wave velocity as a function of test time is ascertained by manual determination of AE velocity from a number of discrete events generated during testing [34].

The distribution of AE energy recorded in the gage section for the coated and uncoated specimens are shown in Figure 6a and 6b respectively. The AE energy is plotted versus its length along the specimen (shown as \pm distance from centerline of the sample). It is worth noting that due to the random distribution of flaws and possible sample degradation, the CMC will experience multiple matrix cracking planes prior to catastrophic failure of the sample. Therefore, it is anticipated that the AE event location analysis will show multiple areas of increased AE activity. Next to the AE histogram for each sample is the associated DIC strain mapping at failure stress. The DIC image of the coated sample at peak load shows a relatively uniform strain mapping with some small areas of elevated strain, which is in good agreement with the recorded

AE data. In particular, the AE energy distribution shows an increased energy region at approximately 10 mm from the centerline correlating with the CMC fracture plane. Similarly, the high energy region near the bottom of the gage section corresponds to the localized high strain region shown in the DIC mapping. The AE energy recorded during the uncoated testing shows a high variation in energy regions, which in turn corresponds to the wide range of strain values seen in the DIC image. The localized regions of increased strain are attributed to unbridged matrix cracking on the specimen surface. As previously discussed, this type of damage morphology is caused by environmental degradation, leading to highly localized stress concentrations. Unlike the coated sample, matrix stresses are not being relieved by load sharing between fibers and matrix at the site of matrix crack formation. Without this load sharing mechanism, the composite exhibits a more elastic failure, similar to a monolithic ceramic material. The uncoated specimen failed outside the area of interest captured by the DIC recording (approximately -30 mm from centerline), however analysis of the AE events near the fracture plane show energy levels several times that seen in the gage section. While the anticipated ultimate fracture plane is within the heated section of the sample, the fact that this specimen failed outside this region was likely caused by highly localized damage resulting from exposure to the burner-rig environment.

Further AE waveform analysis was performed to extract the frequency and energy content of the signals. Figure 7a-b shows the frequency centroid (FC) of each event recorded by both the top and bottom AE sensors. The wave frequency centroid is calculated because it gives a more accurate representation of the frequency content of the entire waveform than peak frequency alone. The FC of damage events in MI SiC/SiC laminates have been shown to be in the in the range of 600 kHz – 1200 kHz [35]. This is clearly consistent with the FC bands seen

for both of the samples tested here. However, Figure 7a shows a dense cluster of low frequency events (270 kHz – 375 kHz), initiating at approximately 125 MPa, not seen in the uncoated sample. Similar frequency content was captured by both the top and bottom sensors throughout the test, including this low frequency cluster. Investigation of the event locations show that they are relatively well dispersed throughout the gage section (Figure 8a). Further examination of this low frequency cluster in Figure 8b, shows that in general these events are all low in relative energy content. The similarity between these events in terms of content (FC and energy) signify that they are likely related to the same type of damage mechanism. It has been shown that AE events related to surface damage generate waveforms dominated by low frequency flexural waves, with a minimal high frequency extensional component [35]. Therefore, this behavior suggests that the low frequency cluster seen in this test are possibly related to EBC cracking that initiated at the applied stress of 125MPa. The frequency content of the uncoated sample (Figure 7b) shows some slightly different behavior. The top and bottom AE sensors show very different FC values for corresponding events, especially at high stresses, where the FC calculated from the AE waveform taken from the bottom sensor is lower than expected for transverse matrix cracking. The proximity of the bottom sensor to the fracture plane could scatter the high frequency content of events occurring closer to the gage section.

4. Conclusions

The capability of using ER measurements for high heat-flux tensile strength testing was demonstrated. The ER measurements used in this study proved to be a valuable tool in determining material damage initiation and accumulation. Furthermore, modal acoustic emission monitoring and digital image correlation were also used in order to investigate material damage state and localized behavior. First, the retained mechanical properties of an uncoated SiC/SiC

CMC and an EBC coated SiC/SiC CMC substrate post-HPBR exposure was investigated. The decreased strength and toughness of the uncoated sample is indicative of oxidation of the composite constituents from exposure to the corrosive burner rig environment. The in-situ ER and AE data showed the differences in damage onset and accumulation between the coated and uncoated samples. Comparison of the ER and AE data shows that while AE measurements are sensitive only to the release of elastic waves generated by cracking events, the change in ER is caused by both matrix cracking and fiber/matrix displacements. Finally, waveform analysis to extract AE energy distributions demonstrated good agreement with DIC strain mapping for determining increased damage regions. Also, comparison of AE event frequency content shows promise in determining EBC crack initiation.

Acknowledgements

This work was supported by the NASA Glenn Research Center, Transformational Tools and Technologies Project. The authors would like to gratefully acknowledge Ron Phillips and Nathan Wilmoth of NASA GRC for their mechanical testing and technical support.

References

- [1] DiCarlo, J.A., Yun, H-M, Morscher, G.N., Bhatt, R.T. SiC/SiC composites for 1200°C and above. In: Bansal NP, editor. Handbook of Ceramics Composites. NY, NY: Kluwer Academic; 2005. p. 77–98.
- [2] Corman, G.S., Luthra, K.L. Silicon melt infiltrated ceramic composites (HiPerComp™). In: Bansal NP, editor. Handbook of Ceramics Composites. NY, NY: Kluwer Academic; 2005. p. 99–115.
- [3] Dicarlo, J. A. Advances in SiC / SiC Composites for Aero-Propulsion Applications. In: N. Bansal and J. Lamon, eds. Ceramic Matrix Composites: Materials, modeling, technology, and applications. Wiley, New York. 2013
- [4] Robinson, R.C., and Smialek, J.L., SiC recession caused by SiO₂ scale volatility under combustion conditions: I, Experimental Results and Empirical Model, J. Am. Ceram. Soc., 82(7) (1999), 1817–1825.
- [5] Opila, E.J., Smialek, J.L., Robinson, R.C., Fox, D.S., and Jacobson, N.S., SiC recession caused by SiO₂ scale volatility under combustion conditions: II, Thermodynamics and gaseous-diffusion model.” J. Am. Ceram. Soc., 82(7) (1999), 1826–1834.
- [6] K.L. More, P.F. Tortorelli, L.R. Walker, N. Miriyala, J.R. Price, M. Van Roode, High-Temperature Stability of SiC-Based Composites in High-Water-Vapor-Pressure Environments, J. Am. Ceram. Soc. 81 (2003) 1272–1281.
- [7] J.L. Smialek, R.C. Robinson, D.S. Fox, N.S. Jacobson, SiC and Si₃N₄ recession due to SiO₂ scale volatility under combustion conditions, Adv. Compos. Mater. 8 (1999) 33–45.
- [8] K.N. Lee, D.S. Fox, N.P. Bansal, Rare earth silicate environmental barrier coatings for SiC/SiC composites and Si₃N₄ ceramics, J. Eur. Ceram. Soc. 25 (2005) 1705–1715.
- [9] Lee, K. N., Fox, D. S., Robinson, R. C., and Bansal, N. P., Environmental barrier coatings for silicon-based ceramics. High temperature ceramic matrix composites, W. Krenkel, R. Naslain and H. Schneider, eds., Wiley, New York, 2001, 224–229.
- [10] D. Zhu, K.N. Lee, R.A. Miller, Thermal Gradient Cyclic Behavior of Thermal and Environmental Barrier Coating Systems on SiC/SiC Ceramic Matrix Composites, IGTI 2002 ASME Turbo Expo, Amsterdam, The Netherlands, 2002.
- [11] Zhu, D., and Miller, R.A. Thermal and environmental barrier coatings for advanced propulsion engine systems, TM-2008-215040, NASA, Washington, DC, 2008.
- [12] Zhu, D., Fox, D.S., Bansal, N.P., and Miller, R.A., Advanced oxide material systems for 1650°C thermal/environmental barrier coating applications, TM-2004-213219, NASA, Washington, DC, 2004.
- [13] Zhu, D., Miller, R.A., and Fox, D.S., Thermal and environmental barrier coating development for advanced propulsion engine systems, 2007-2130 (NASA/TM-2008-215040), American Institute of Aeronautics and Astronautics, Reston, VA, 2007.

- [14] Zhu, D., Miller, R.A., Multifunctionally graded environmental barrier coatings for silicon-based ceramic components, US Patent No. 7740960 B1, June 22, 2010.
- [15] Halbig, M.C., Jaskowiak, M.H., Kiser, J.D. and Zhu, D., Evaluation of Ceramic Matrix Composite Technology for Aircraft Turbine Engine Applications, 51st AIAA Aerospace Sciences Meeting including the New Horizons Forum and Aerospace Exposition, AIAA 2013-0539, 2013.
- [16] R. Naslain, Design, preparation and properties of non-oxide CMCs for application in engines and nuclear reactors: an overview, *Compos. Sci. Technol.* 64 (2004) 155–170.
- [17] Fox, D.S., Miller, R.A., Zhu, D., Perez, M., Cuy, M.D., and Robinson, R.C., Mach 0.3 Burner Rig Facility at the NASA Glenn Materials Research Laboratory. NASA/TM-2011-216986, 2011.
- [18] M. van Roode, J. Price, J. Kimmel, N. Miriyala, D. Leroux, A. Fahme, et al., Ceramic Matrix Composite Combustor Liners: A Summary of Field Evaluations, *J. Eng. Gas Turbines Power.* 129 (2007).
- [19] G.S. Corman, a. J. Dean, S. Brabetz, M.K. Brun, K.L. Luthra, L. Tognarelli, et al., Rig and Engine Testing of Melt Infiltrated Ceramic Composites for Combustor and Shroud Applications, *J. Eng. Gas Turbines Power.* 124 (2002) 459–464.
- [20] D. Zhu, R.A. Miller, B.A. Nagaraj, R.W. Bruce, Thermal conductivity of EB-PVD thermal barrier coatings evaluated by a steady-state laser heat flux technique, *Surf. Coatings Technol.* 138 (2001) 1–8.
- [21] B.D. Choules, K. Kokini, T.A. Taylor, Thermal fracture of ceramic thermal barrier coatings under high heat flux with time-dependent behavior. Part 1. Experimental results, *Mater. Sci. Eng. A.* 299 (2001) 296–304.
- [22] C. Smith, G. Morscher, Z. Xia, Monitoring damage accumulation in ceramic matrix composites using electrical resistivity, *Scr. Mater.* 59 (2008) 463–466.
- [23] G.N. Morscher, C. Baker, C. Smith, Electrical Resistance of SiC Fiber Reinforced SiC/Si Matrix Composites at Room Temperature during Tensile Testing, *Int. J. Appl. Ceram. Technol.* 11 (2014) 263–272.
- [24] Appleby, M., Morscher, G. N., and Zhu, D., Creep and Environmental Durability of Environmental Barrier Coatings and Ceramic Matrix Composites under Imposed Thermal Gradient Conditions, 37th International Conference and Expo on Advanced Ceramics and Composites, Daytona Beach, FL, 2013.
- [25] G.N. Morscher, V. V. Pujar, Design Guidelines for In-Plane Mechanical Properties of SiC Fiber-Reinforced Melt-Infiltrated SiC Composites, *Int. J. Appl. Ceram. Technol.* 6 (2009) 151–163.
- [26] D. Zhu, Development and Performance Evaluations of HfO₂-Si and Rare Earth-Si Based Environmental Barrier Bond Coat Systems for SiC / SiC Ceramic Matrix Composites NASA EBC and CMC System Development, 41st Int. Conf. Metall. Coatings Thin Film., San Diego, CA, 2014.

- [27] D. Zhu, J. Hurst, Advanced High Temperature and Fatigue Resistant Environmental Barrier Coating Bond Coat Systems for SiC/SiC Ceramic Matrix Composites, US Patent No. 20130344319, 2013.
- [28] D. Zhu, B.A. Sakowski, C. Fisher, Film Cooled Recession of SiC/SiC Ceramic Matrix Composites: Test Development, CFD Modeling and Experimental Observations, 41st Int. Conf. Metall. Coatings Thin Films. San Diego, CA, April 28-May 2, 2014.
- [29] J. Aveston, G.A. Cooper, A. Kelly, Single and Multiple Fracture, Natl. Phys. Lab. (1971).
- [30] J.W. Hutchinson, H.M. Jensen, Models of Fiber debonding and Pullout in Brittle Composites with Friction, Mech. Mater. 9 (1990) 139–163.
- [31] D.B. Marshall, Analysis of Fiber Debonding and Sliding Experiments in Brittle Matrix Composites, Acta Met. Mater.. Mater. 40 (1992) 427–441.
- [32] G. N. Morscher. Tensile stress rupture of SiCf/SiCm minicomposites with carbon and boron nitride interphases at elevated temperatures in air. J. Am. Ceram. Soc., 80(8), 2029–2042 (1997)
- [33] G.N. Morscher, Stress-dependent matrix cracking in 2D woven SiC-fiber reinforced melt-infiltrated SiC matrix composites, Compos. Sci. Technol. 64 (2004) 1311–1319.
- [34] G.N. Morscher, Modal acoustic emission of damage accumulation in a woven SiC / SiC composite, Compos. Sci. Technol. 59 (1999) 687–697.
- [35] E. Maillet, G.N. Morscher, Waveform-based selection of acoustic emission events generated by damage in composite materials, Mech. Syst. Signal Process. 52-53 (2015) 217–227.

Table I: SiC/SiC specimen geometry, fiber content (f_0), and room-temperature electrical properties pre-tensile testing

Specimen	width (mm)	Thickness (mm)	f_0	Electrical Resistance (ohm)	
				Room temp.	Test temp.
coated	12.80	2.25	0.143	0.61985	1.0150
uncoated	12.72	2.21	0.145	0.73418	1.1726

Table II: Conditions and mechanical properties of test samples during high-temperature tensile testing.

Specimen	Surface Temp. (°C)	Back Temp. (°C)	E (GPa)		σ_{UTS} (MPa)	ϵ_{fail} (%)	AE onset stress (MPa)
			Extensometer	DIC			
coated	1230	1070	241	266	238	0.371	149
uncoated	1200	1010	146	221	166	0.134	115

List of Figure Captions

Fig. 1. Image of tensile loading frame with incorporated high heat-flux laser heating and digital image correlation (DIC) apparatus used for high temperature tensile strength testing.

Fig. 2. Schematic of high-temperature tensile test setup; including configuration of electrical resistance (ER) electrodes and modal acoustic emission (AE) sensors.

Fig. 3. Mechanical behavior of samples under high temperature monotonic tensile loading, post environmental exposure. Strain measurement taken from high temperature extensometer, as well as from contact points of extensometer probes as observed from DIC images (includes thermal and mechanical strain).

Fig. 4. High temperature retained tensile strength test: (a) comparison of in-situ electrical resistance (ER) and acoustic emission (AE), and (b) change of ER with nominal mechanical strain.

Fig. 5. In-situ electrical resistance versus normalized cumulative AE energy (approximate normalized matrix cracking) during high temperature tensile tests of (a) coated and (b) uncoated samples.

Fig. 6. Distribution of AE event energy along the gage length and associated DIC strain mapping of gage (at failure stress) during high temperature tensile testing for the (a) coated and (b) uncoated sample respectively.

Fig. 7. Stress-dependent AE events recorded by each sensor during high temperature monotonic tensile testing, showing calculated frequency centroid for the (a) coated sample (with low frequency cluster highlighted), and (b) uncoated sample, respectively.

Fig. 8. AE events during high temperature testing of coated sample with (a) gage- length location of events identified in low frequency (270 kHz – 375 kHz) cluster, (b) Average AE event energies with low frequency events highlighted.

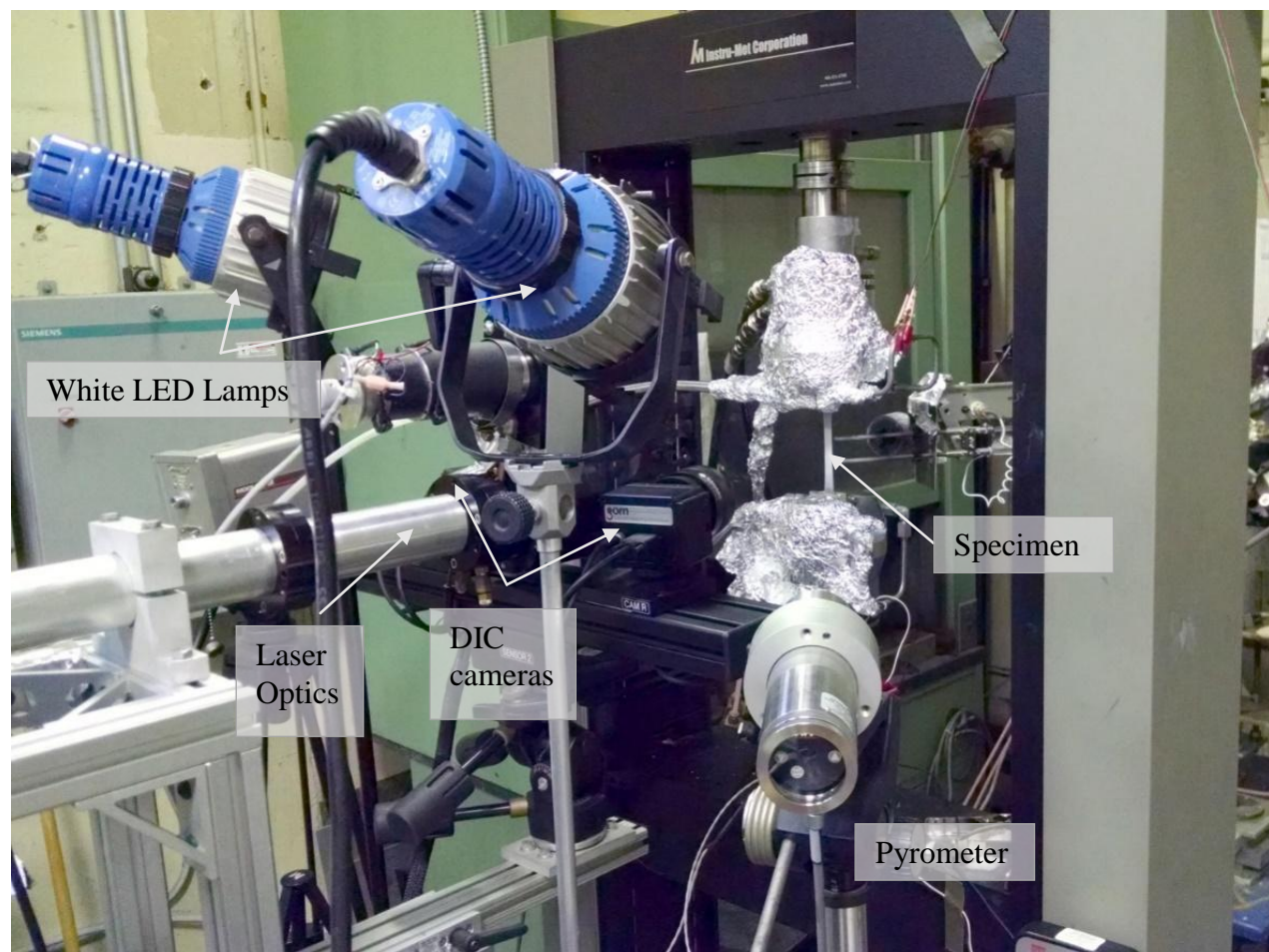


Fig. 1.

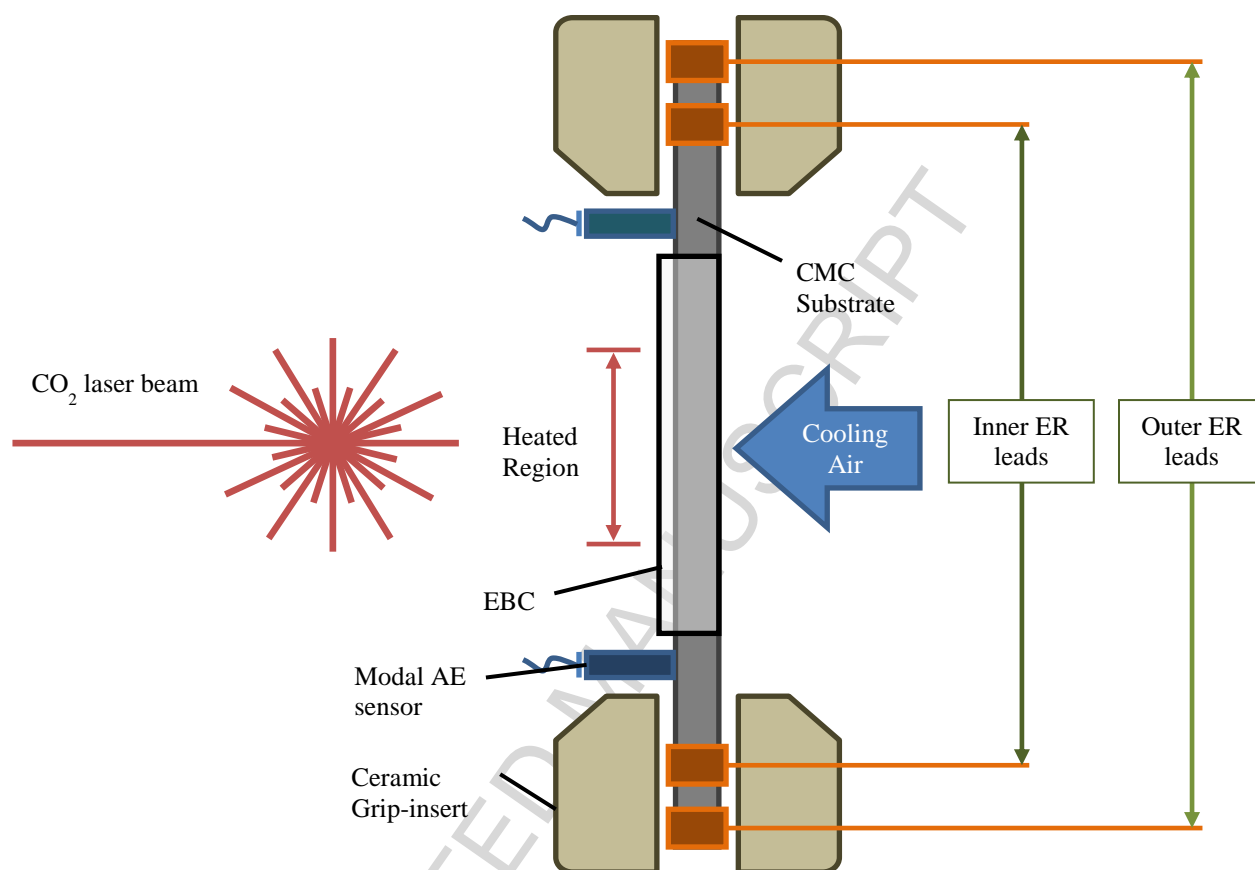


Fig. 2.

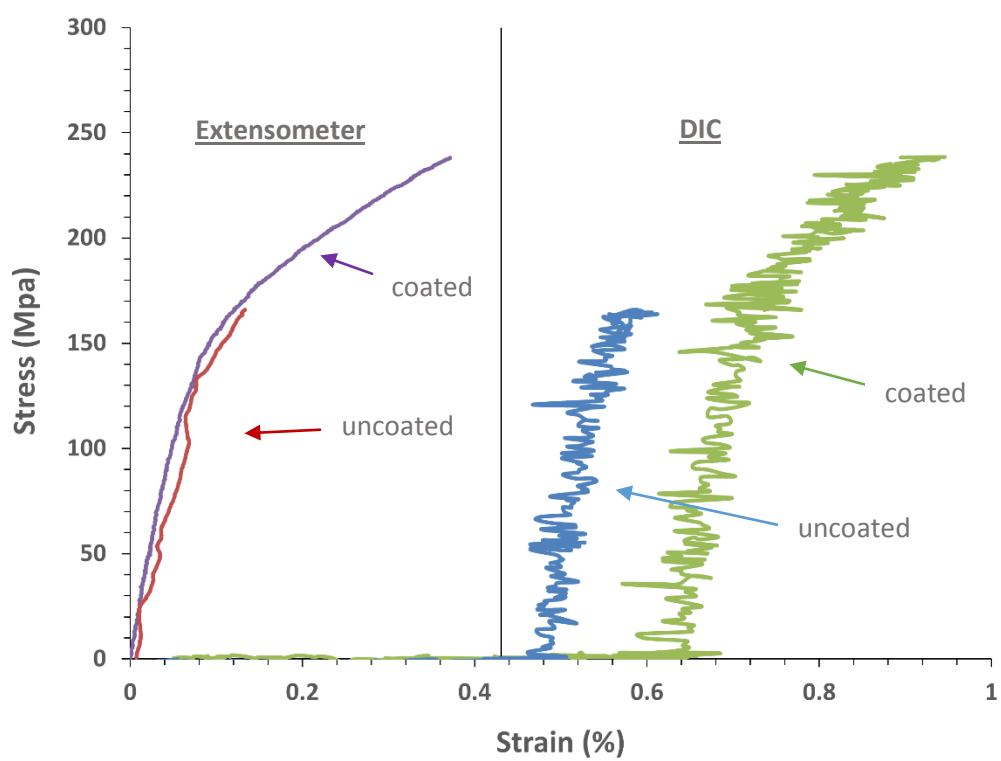
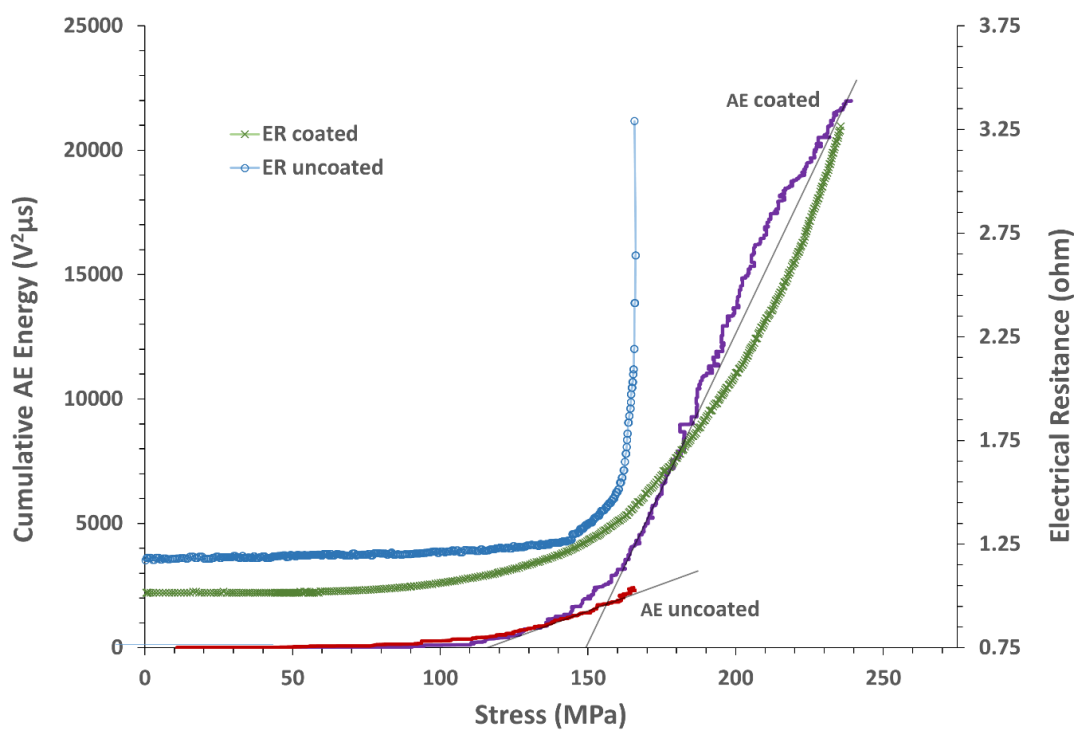
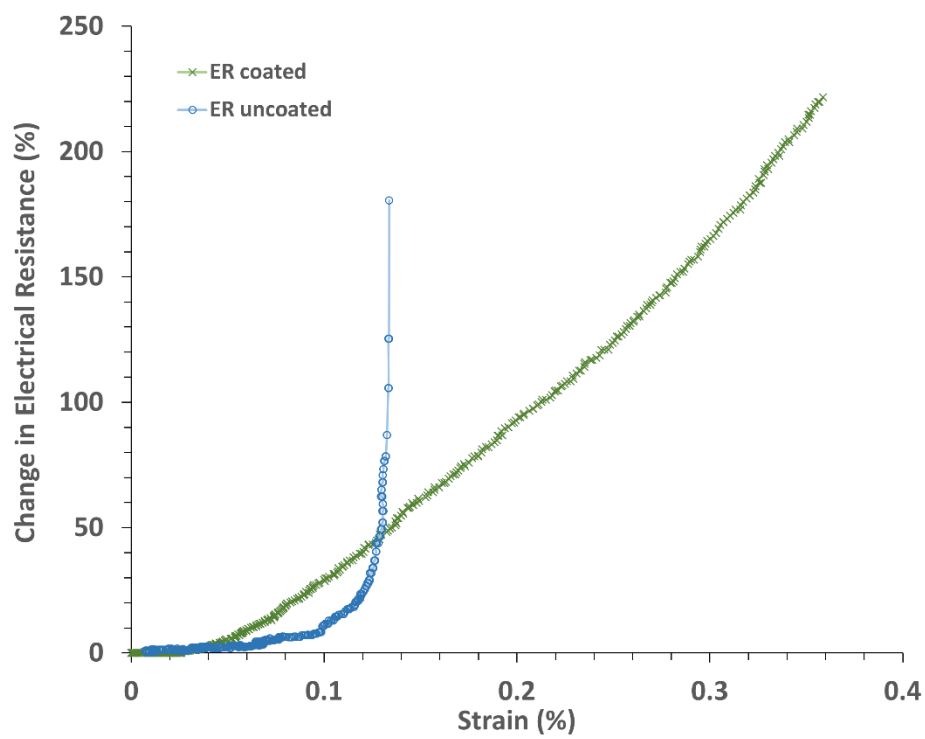


Fig. 3.

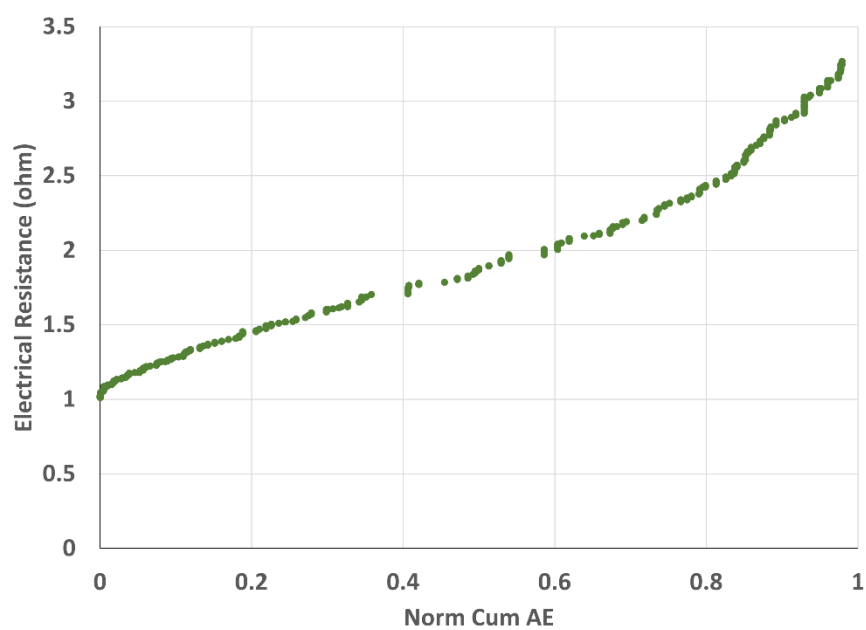


(a)

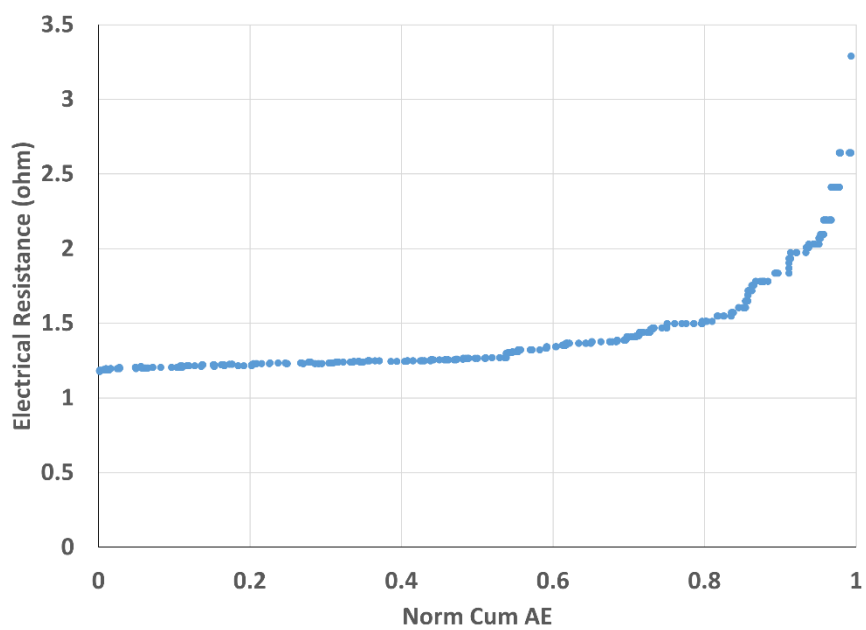


(b)

Fig. 4.

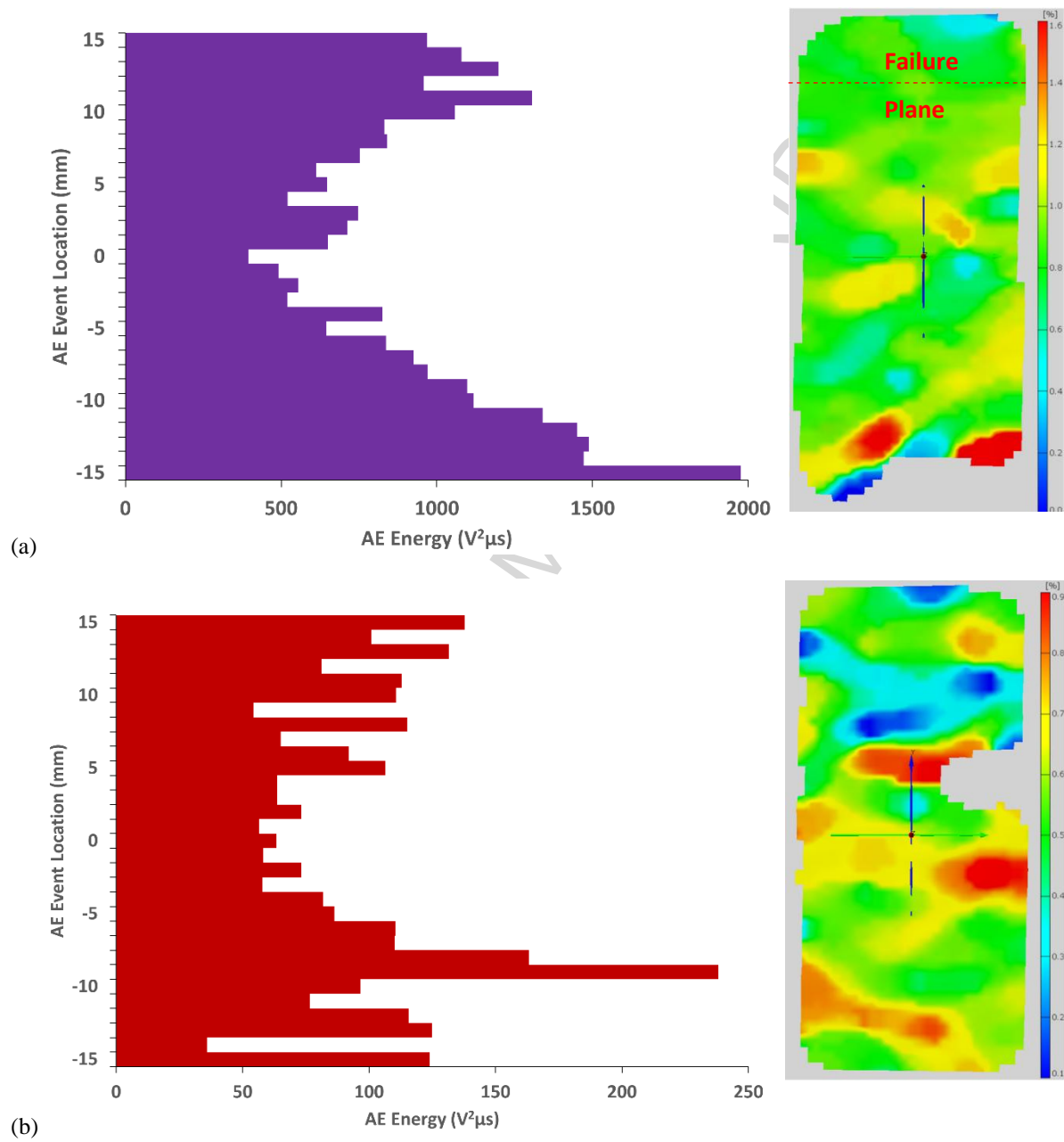


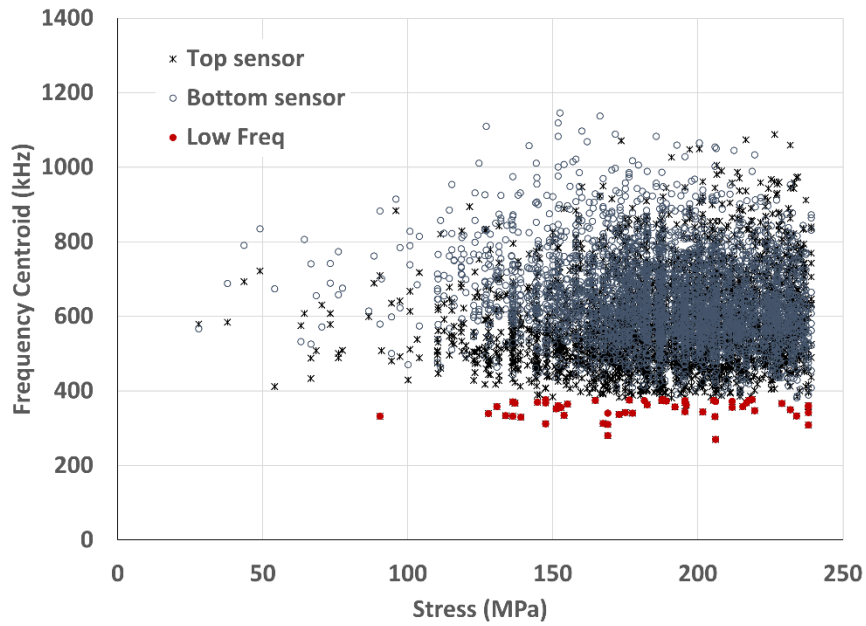
(a)



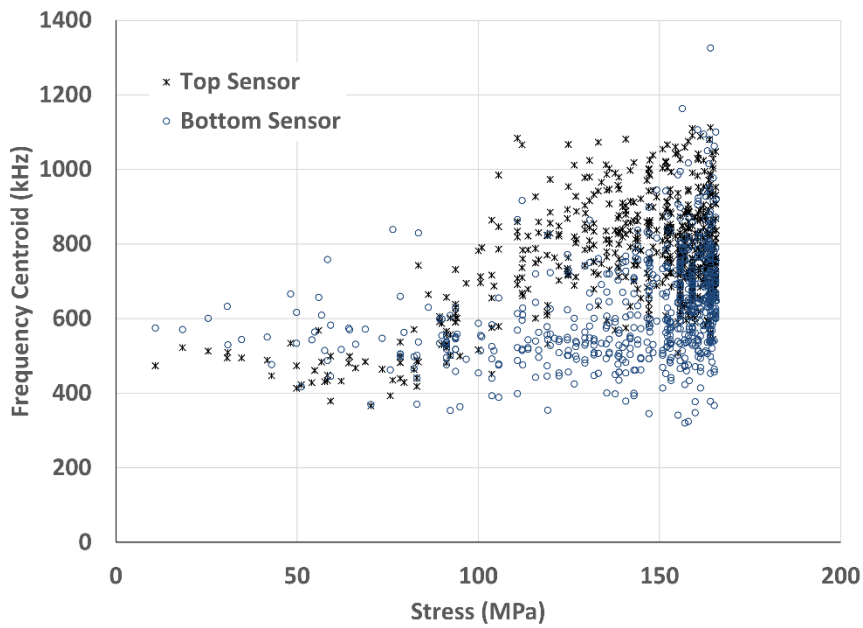
(b)

Fig. 5.

**Fig. 6.**

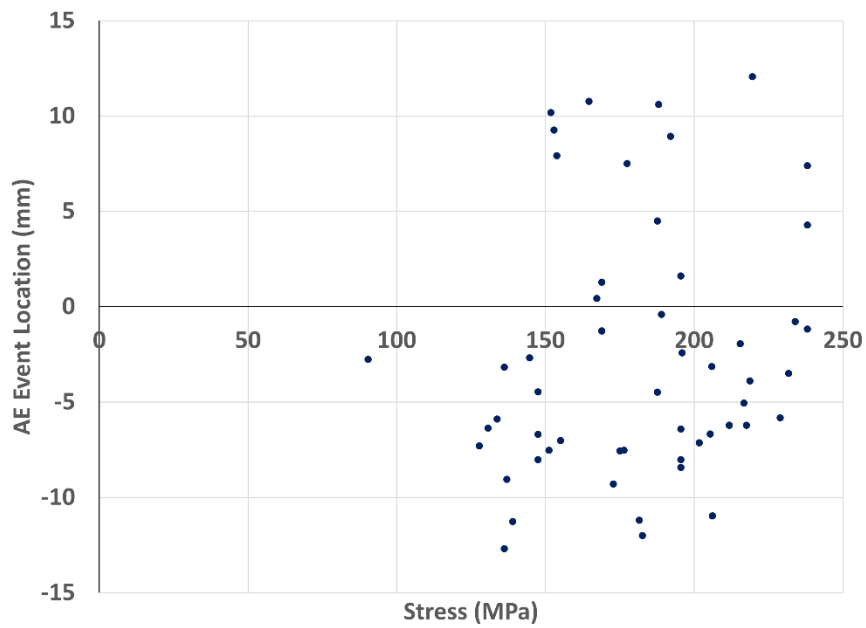


(a)

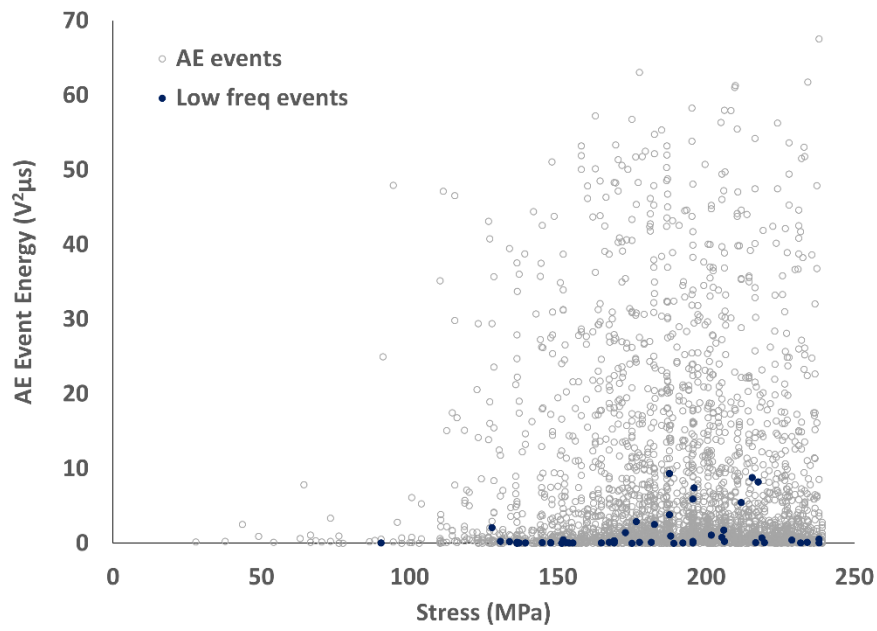


(b)

Fig. 7.



(a)



(b)

Fig. 8.

Highlights

- Decrease in retained tensile properties post HPBR exposure clearly shows degradation of uncoated specimen, and in turn the increased performance benefit of the NASA EBC system
- ER measurement shown to be an effective tool for in-situ damage monitoring of MI SiC/SiC CMCs under high-temperature thermal gradients
 - Damage onset indicated by steep ER increase in both cases
 - Increases in ER response show high sensitivity (100's of % increase to failure)
- AE energy analysis showed good agreement with DIC strain mapping in terms of damage location and distribution
- AE waveform analysis revealed some differences in frequency content and energy between the coated and uncoated samples
 - While further study is required, there is evidence that AE analysis can be used to more clearly differentiate EBC from CMC damage events